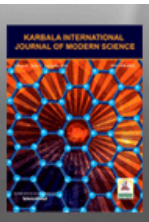

Karbala International Journal of Modern Science

Volume 7 | Issue 4 Article 7

Biosynthesis, characterization and antiproliferative activity of green synthesized gold nanoparticles using Lantadene A extracted from Lantana camara

Dawood Ali Salim Dawood
School of Biomedical Engineering and Health Science, Faculty of Engineering, Universiti Teknologi Malaysia and Branch of Forensic Medicine and Pathology, College of Medicine, University of Wasit, Iraq

Lee Suan Chua Ph.D
Department of Bioprocess and Polymer Engineering, School of Chemical and Energy Engineering, Faculty of Engineering, Universiti Teknologi Malaysia, and Institute of Bioproduct Development, Universiti Teknologi Malaysia, chualeesuan@utm.my

Tian Swee Tan Ph.D
School of Biomedical Engineering and Health Science, Faculty of Engineering, Universiti Teknologi Malaysia

Ahmed F. Alshemary Ph.D
Biotechnology Research Center, Al-Nahrain University, Baghdad, Iraq

Biosynthesis, characterization and antiproliferative activity of green synthesized gold nanoparticles using Lantadene A extracted from Lantana camara

Abstract

This study was focused on the biosynthesis of gold nanoparticles loaded with lantadene A (LA-AuNPs) from Lantana camara extract and the antiproliferative effects on prostate cancer cells (LNCaP). The synthesized LA-AuNPs had smooth surface, and nearly spherical in shape (67.94 nm) with the zeta potential (-30.11±0.83 mV). LAAuNPs showed a dose dependent cytotoxic activity with IC50, 126.82 µg/mL against LNCaP, but non-cytotoxic to normal prostate cells. The intrinsic pathway of apoptosis was caused by the increase of caspases-3/7 and -9 activity and cell cycle arrest at the G0/G1 phase. Therefore, LA-AuNPs could be a potent lead to inhibit LNCaP

Keywords

gold nanoparticles, green synthesis, lantadene A, anti-cancer

1. Introduction

Nanotechnology enables the synthesis of nanoscale substances, approximately less than 100 nm [1,2]. One of the challenges is developing an effective experimental protocol to synthesize nanoparticles with consistent and well characterized physiochemical properties including high mono-dispersity in particle size [3].

The concept of environmental safety and green technology has been the key consideration in nanotechnology development [4,5]. Recently, the development of metallic nanoparticles such as gold, silver, titanium, platinum, cerium, iron, thallium and zinc has attracted much attention, mainly due to the unique catalytic, optical and magnetic properties of metals [6]. The use of low-cost and eco-friendly materials is considered as the green synthesis for metallic nanoparticles. For the last decade, gold nanoparticles (AuNPs) has been considered to be the best drug carrier due to the excellent and unique properties like controlled size, biocompatibility, stability and safer than other metallic nanoparticles [7,8]. Therefore, AuNPs have been applied in several applications such as, anti-cancer, antimicrobial and anti-inflammation [9]. There were also studies reported on the incorporation of different phytochemicals in AuNPs [10−13]. Phytochemicals like saponins, terpenes, alkaloids, phenolics, carbohydrates and lipids may reduce metallic ions during nanoparticle synthesis [14]. Previous studies mentioned the synthesis and characterization of different metallic NPs [15−17] including AuNPs [18−20] using various extracts from different parts of *Lantana camara*. *L. camara* is one of famous ornamental and herbal shrubs belonging to the family Verbenaceae. *L. camara* is commonly grows in subtropical, tropical and temperate areas [21]. It is also known as Spanish flag, Surinam Tea Plant and red sage [22] with different flower color such as violet, red, pink, yellow and white. Numerous phytochemicals were extracted and identified from different parts of *L. camara* including steroids, iridoid, flavonoids, glycosides, steroids, phenylpropanoid glycosides, oligosaccharides, naphthoquinones and triterpenoids. Lantadene A (LA) (22β-angeloyloxy-3-oxoolean-12-en-28-oic acid) is a pentacyclic triterpenoid which is a dominant compound in *L. camara* leaves [23,24].

The phytochemical synthesized metallic nanoparticles have been reported to be more feasible and stable in nanomedicine applications. Therefore, scientists are encouraged to develop a new, safer and effective drug delivery system to treat various types of cancers. In particular, prostate cancer represents the second most common cancer and the fifth most common cause of cancer death in men worldwide [25].

In the present study, the active compound, LA was extracted from *L. camara* and reacted with gold to form LA-AuNPs. The green-synthesized (LA−AuNPs) were characterized for their physiochemical properties such as chemical stability, elemental composition, particle size, zeta potential and surface morphology for better understanding the role of LA-AuNPs in prostate cancer cell treatment. The characteristics were interpreted with the observation of high cell screening, caspase activity and cell cycle arrest phenomenon to explain the apoptosis pathway. The cytotoxicity of LA-AuNPs against LNCaP was also compared with prostate normal cell line.

2. Materials and methods

2.1. Chemicals, cell lines and plant material

L. camara leaves were collected from the garden of Baghdad University (Al-Jadriya, Baghdad, Iraq). The authentication of the plant was carried out by Dr. Zainab Abid Aun from the Department of Biology, College of Sciences for Women, Baghdad University (Baghdad, Iraq) and processed by Mr. Ikhlas Hussain Alwan who is a researcher of from the National Herbarium, Ministry of Agriculture (Baghdad, Iraq). The specimen has been deposited at the National Herbarium, Ministry of Agriculture (Baghdad, Iraq) with the registration number of 1169. The prostate cancer cell line (LNCaP) and prostate normal cell line (RWPE-1) were purchased from American Type Culture Collection, ATCC (Manassas, Virginia, USA). Roswell Park Memorial Institute Medium (RPMI 1640), keratinocyte serum free medium (K-SFM) and gold(III) chloride trihydrate ($HAuCl_4.3H_2O$), dimethyl sulfoxide (DMSO) and 3-(4,5-dimethylthiazol-2-yl)-2,5-diphenyltetrazolium bromide (MTT) were purchased from Sigma−Aldrich (St. Louis, MO, USA). Acetic acid, methanol, chloroform and acetonitrile were obtained from Merck (Darmstadt, Germany).

https://doi.org/10.33640/2405-609X.3158

2.2. Extraction and purification of lantadene A

The collected leaves were dried and then ground into powder. The leaf powder (100 g) was mixed with 500 mL methanol and macerated for 24 h with intermittent shaking at 30 °C. The extract was filtrated using muslin cloth and decolorized with 20 g activated charcoal to obtain a yellowish solution.

The methanol solution was concentrated by evaporation and reconstituted in a methanol–water (1:7) mixture (15 mL). The solution was extracted with chloroform by vigorous shaking in a 100 mL separating funnel. The chloroform layer was withdrawn after extraction. Another fresh chloroform (15 mL) was added into the remaining aqueous solution for vigorous shaking again. The organic layer was then collected and combined prior to dehydration by adding a small amount of anhydrous sodium sulphate. The organic layer was then concentrated by a rotary evaporator.

The concentrated residue was added into 100 mL methanol and left for crystallization. The obtained white crystal (1.06 g) was reconstituted in methanol and chromatographed through a silica gel packed column (30 g, 60–120 mesh) using the solvent system of chloroform–methanol (99.5:0.5). The eluted solution was concentrated *in vacuo* again and recrystallized in methanol to form pure lantadene A (0.45 g).

2.3. Biosynthesis of lantadene A loaded gold nanoparticles (LA-AuNPs)

The green synthesis of LA-AuNPs was performed according to the previously reported procedures with slight modification [26]. A 2 mL aqueous $HAuCl_4 \cdot 3H_2O$ (1 mM) was added dropwise to 10 mL of LA (1 mg/mL) with a constant stirring speed at 70 °C for 5–80 min. A gradual change of color was observed which indicated that LA was incorporated with gold nanoparticles. The UV–Vis absorption spectrum was reported as a function of time to monitor the progress of $AuCl^{4-}$ reduction. The absorbance of sample was monitored using an UV–Vis spectrophotometer at the scan range of 400–1100 nm (UV-1800, Shimadzu, Tokyo, Japan). The mixture of synthesized LA-AuNPs was centrifuged at 16,000 rpm for 15 min. The residue was washed three times with deionized water and then left to drying.

2.4. Cytotoxicity assay

LNCaP cells were cultured in RPMI 1640 supplemented with 10% FBS, 100 U/mL penicillin and 100 μg/mL streptomycin. RWPE-1 cells were grown in K-SFM supplemented with recombinant epidermal growth factor and bovine pituitary extract. All cells were incubated in 5% CO_2, 37 °C for 3–5 days until reached 80–90% confluency.

MTT assay was carried out to determine the cell viability of LNCaP and RWPE-1 after treated with different concentrations of LA-AuNPs ranged from 6.25 to 400 μg/mL. DMSO was used as negative control. Briefly, 1×10^5 cells/well were seeded in a 96-well plate and incubated overnight in 5% CO_2, 37 °C to obtain 80–90% confluency. The cells were then treated with LA-AuNPs and further incubated for 24 h. A 50 μL of MTT (2 mg/mL) was added to the treated cells and incubated for another 2 h. After incubation, the formazan crystals were removed by DMSO. The viability of cells was determined at 570 nm using an ELISA microplate reader (Bio-Rad, Hercules, California, USA). The results are expressed in growth inhibition as calculated using equation (1).

$$\text{Growth inhibition}(\%) = \frac{\text{Optical density of treated sample}}{\text{Optial density of DMSO(contol)}} x100 \quad (1)$$

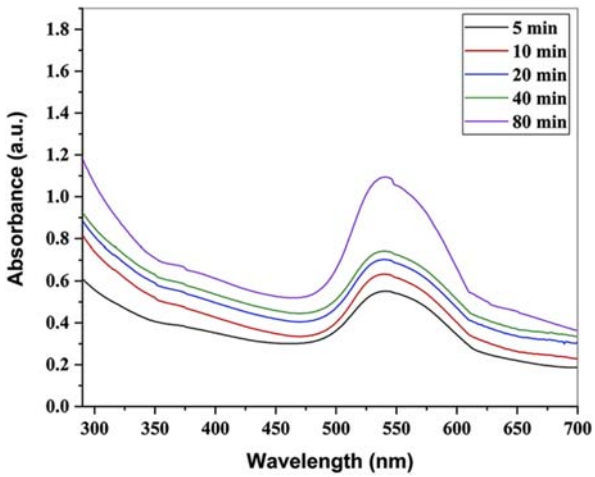

Fig. 1. UV–vis absorption spectra of the formed LA-AuNPs.

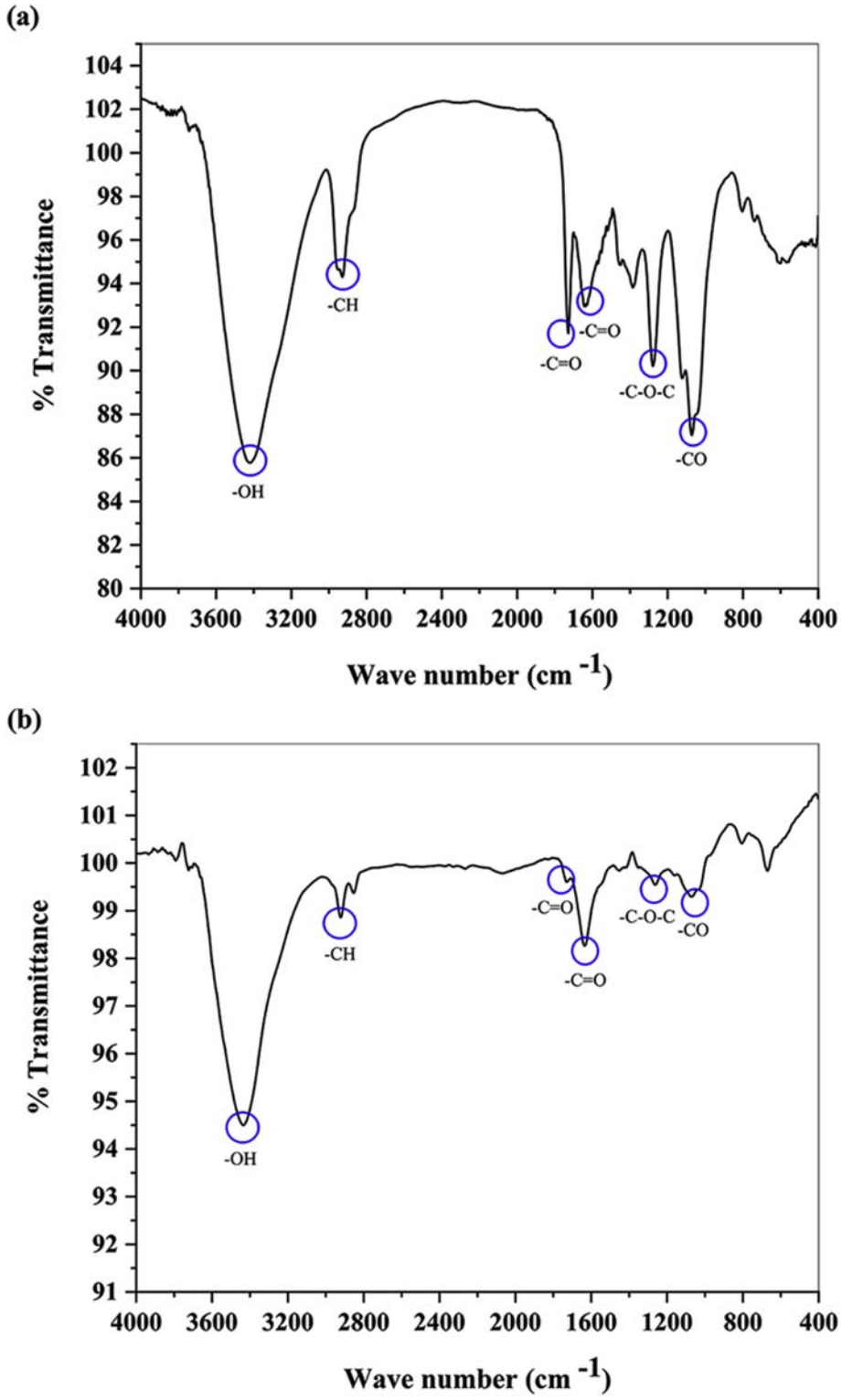

Fig. 2. FTIR spectra of (a) LA and (b) synthesized LA-AuNPs.

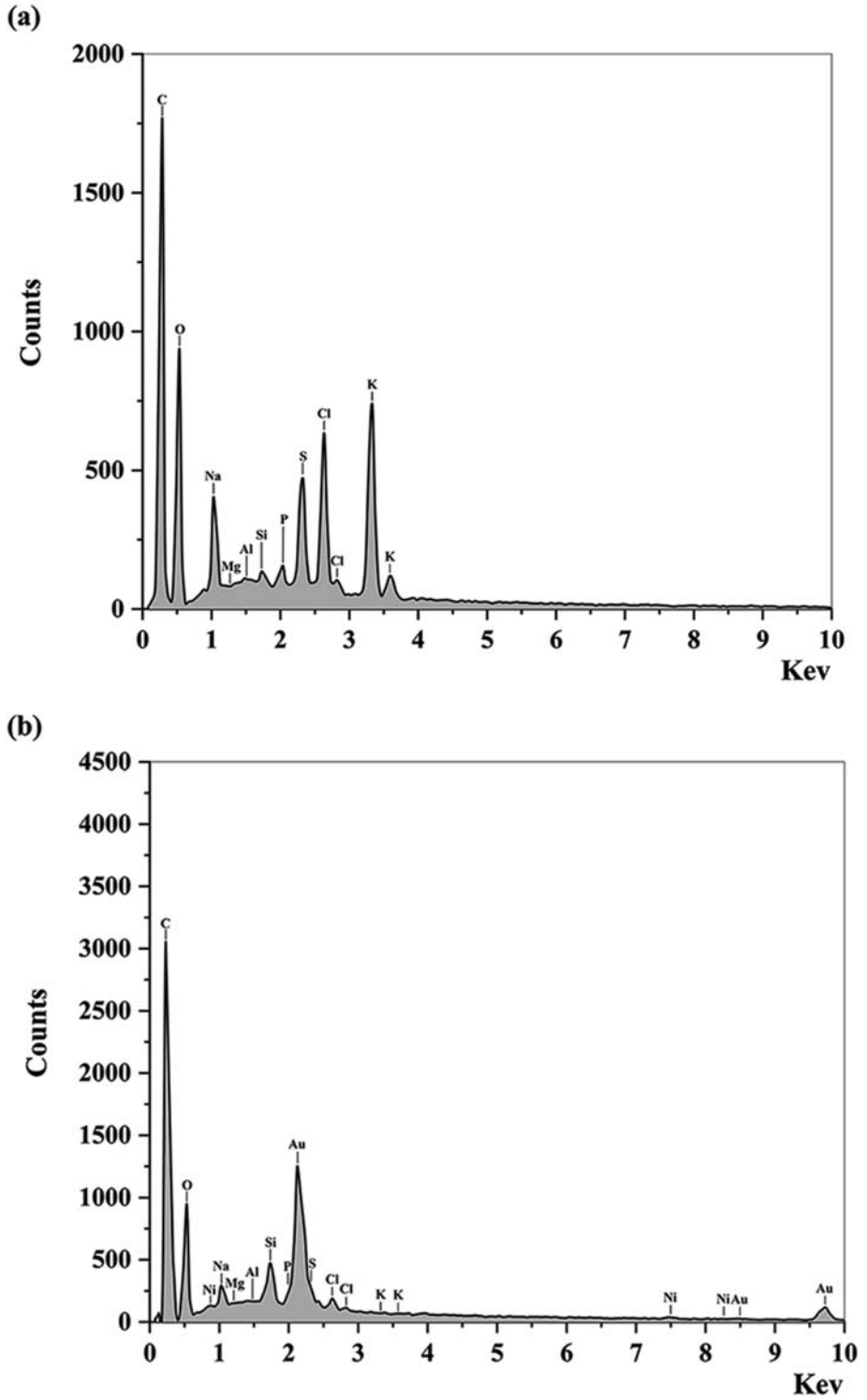

Fig. 3. EDX profiles of (a) LA and (b) crystalline LA-AuNPs.

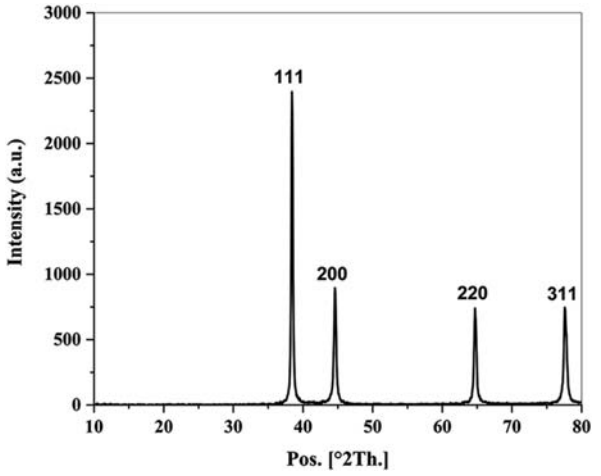

Fig. 4. X-ray diffraction (XRD) profile of crystalline LA-AuNPs.

The IC50 is defined as the required concentration of LA-AuNPs to inhibit 50% cell viability. The experiment was carried out in triplicate.

2.5. High content screening

Cellomics multiparameter cytotoxicity 3 kit (Thermo Scientific™, Pittsburgh, PA, USA) was used to evaluate cell nuclear intensity, cell membrane permeability, mitochondrial membrane potential (MMP) and cytochrome C release after treated with LA-AuNPs. After 24 h of treatment, cell permeability dye and MMP dye were added to the cells (1×10^4 cells/well) and incubated for 30 min at 37 °C. Blocking buffer ($1 \times$) was used in the fixation and permeabilization of cells. Cells were probed with primary cytochrome C antibody and secondary DyLight 649 conjugated with goat anti-mouse immunoglobulin G for 1 h each. The staining solution was supplemented with Hoechst 33,342 to stain the nucleus of cells. The analysis was performed using the ArrayScan high content screening system (Cellomics, PA, USA).

2.6. Measurement of caspase-3/7, −8 and −9 activities

The activities of caspase-3/7, −8 and −9 were determined using Caspase-Glo-3/7, −8 and −9 kit (Promega, Madison, WI, USA), according to the manufacture's protocols. Initially, cells (1×10^4 cells/well) were seeded and treated with LA-AuNPs overnight. DMSO was used as the negative control. The next day, 100 μL of caspase-Glo reagent was added to the each well and then incubated for 30 min. The activities of samples were measured using a Tecan Infinite® 200 Pro (Tecan, Männedorf, Switzerland) microplate reader. The experiment was repeated in triplicate.

2.7. Cell cycle arrest analysis

The cell cycle was evaluated using a flow cytometer (BD Biosciences, New Jersey, USA). Approximately, 1×10^5 cells/well were seeded and treated with LA-AuNPs for 24 h. DMSO was used as negative control. The treated cells were then washed twice with PBS. The cells were fixed using 70% cold ethanol. The cells were stained with PI supplemented with RNase. The percentage of cells were measured in (G0/G1, S and G2/M) phases.

2.8. High performance liquid chromatography

The white crystal was then dissolved in methanol for HPLC (Shimadzu LC-2010A HT, Kyoto, Japan) analysis at 240 nm. The separation was carried out using a Phenomenex C18 column (4 μm, 150 × 4.6 mm) at the isocratic gradient. The mobile phase was consisted of methanol: acetonitrile: water: acetic acid (68:20:12:0.1). The flow rate was 1.2 mL/min and the injection volume was 20 μL.

2.9. Characterization of LA-AuNPs

LA-AuNPs were evaluated for the chemical stability of LA based on its functional groups using Fourier transform infrared spectroscopy (FTIR, IRPrestige-21, Shimadzu, Tokyo, Japan). A small amount of sample was homogenized with KBr and the mixture was analyzed at the spectral range of 4000-400 cm^{-1}. The crystalline nature of LA-AuNPs was analyzed using a X-ray diffractometer (XRD- 6000, Shimadzu, Tokyo, Japan) which was operated at 45 kV and 40 mA with Kα for Cu ($\lambda = 1.54$ Å) and the scanning was performed at $2\theta = 10°-80°$ angles. The mean of crystallite size was calculated using Scherrer equation (2) based on the average of four reflection peaks; 38.417° (111), 44.603° (200), 64.725° (220) and 77.618° (311).

$$D = \frac{k\lambda}{\beta cos\theta} \quad (2)$$

D: mean of crystallite size
k: a dimensionless shape factor of 0.9
λ: X-ray wavelength
β: full width at half maximum of peak (radians) corrected for instrumental broadening.

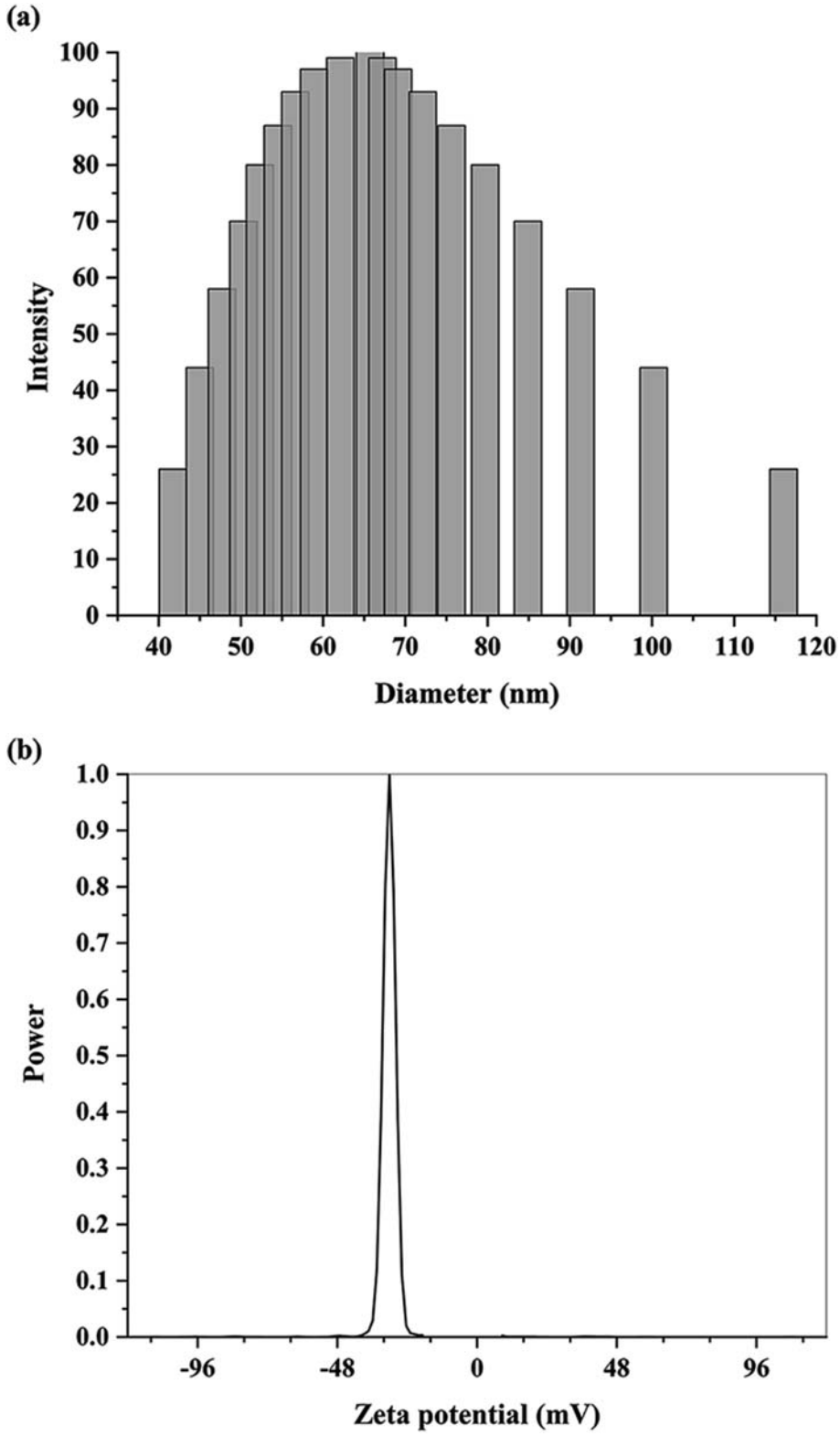

Fig. 5. (a) Dynamic light scattering for particle size distribution based on light intensity and (b) zeta potential of LA-AuNPs.

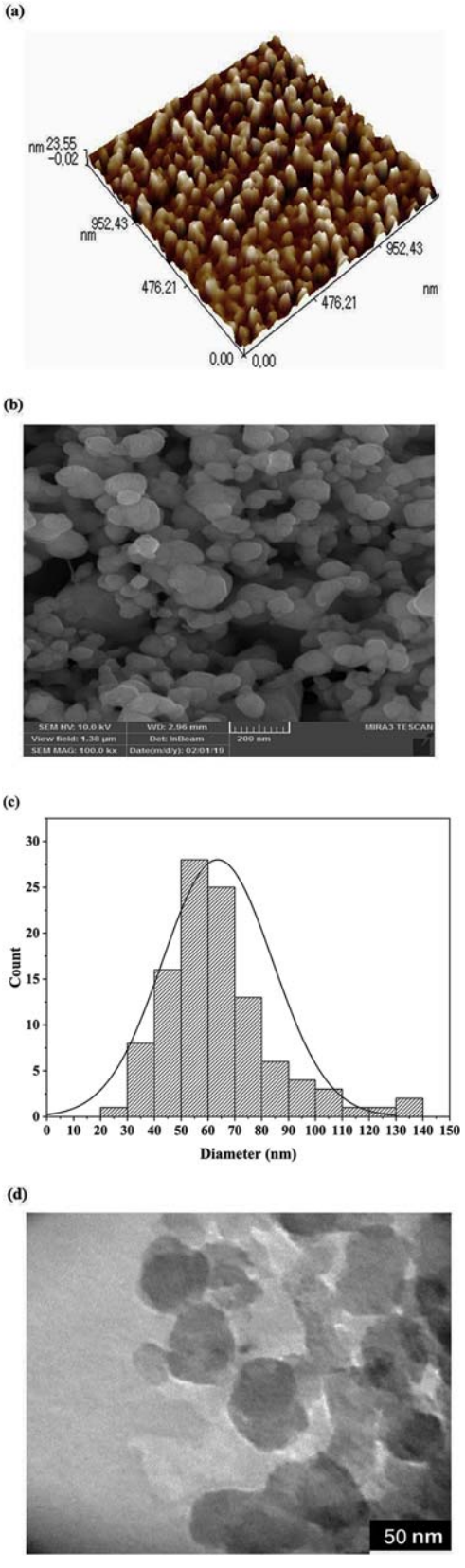

θ: the Bragg diffraction angle obtained from 2θ value corresponding to maximum intensity peak (radians).

The analysis of elements was performed using a X-Max 50 energy dispersive X-ray spectrometer (EDX; Oxford Instrument, Abingdon, UK) coupled with a scanning electron microscope (SEM). The particle size distribution (light intensity) and polydispersity index of LA-AuNPs, as well as the surface electrical charge (zeta potential) were estimated to determine the colloidal stability using a zeta analyzer (ZetaPlus, Brookhaven, NY, USA). The sample was sonicated before test to avoid any possible aggregation.

The surface roughness, surface morphology and particle size were also carried out using a combined atomic force microscopy (AFM) and scanning probe microscope (AA3000 SPM, Angstrom Advanced, Inc., Stoughton, MA, USA). Further morphological analysis of synthesized LA-AuNPs was conducted using a field emission scanning electron microscope (MIRA 3 FESEM, TESCAN, Brno, Czech Republic) and transmission electron microscopy (JEM-2100 TEM, JEOL Ltd., Tokyo, Japan) operated at 200 kV. The frequency histogram of particle size distribution was analyzed using ImageJ (version 1.53 k, Maryland, USA).

2.10. Statistical analysis

The results were expressed as mean ± standard deviation. ANOVA was performed to determine the significance of results using GraphPad Prism 7 (La Jolla, CA, USA). The statistical significance is defined at $p \leq 0.05$.

3. Results and discussion

3.1. Physiochemical characterisation of LA-AuNPs

The addition of LA into the gold ion solution caused the gradual change of color solution from pale yellow into ruby-red. This indicated the reduction of gold ions (Au^{3+}) to gold nanoparticles. The color change can be explained by the excitation of surface plasmon resonance [27]. The biosynthesis and fabrication of nanoparticles was also monitored using an UV–Vis spectrophotometer in a time dependent manner (Fig. 1). The UV–Vis spectra of synthesized AuNPs showed a strong surface plasmon resonance

Fig. 6. (a) 3D AFM images, (b) SEM, (c) histogram of particles size distribution and (d) TEM showing the surface topology of LA-AuNPs.

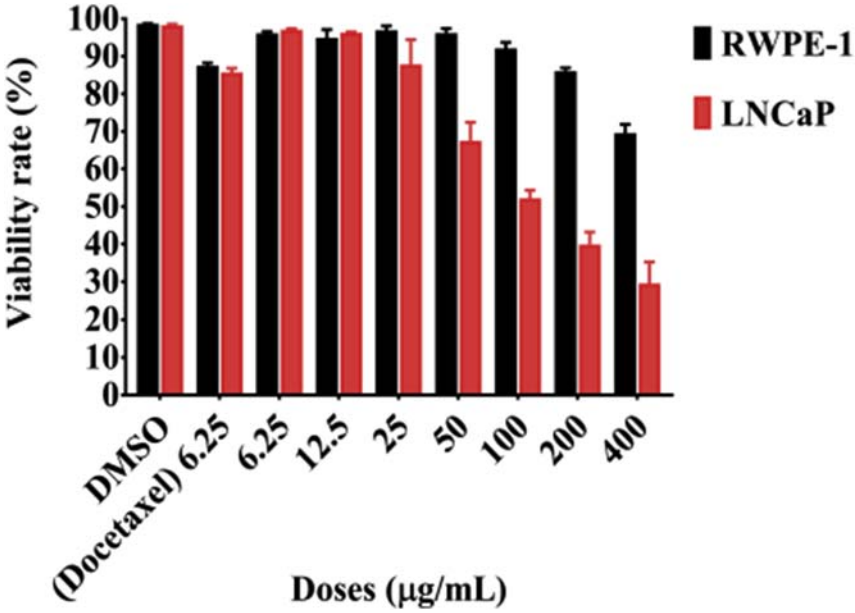

Fig. 7. Percentage growth of LNCaP and RWPE-1 cells treated by LA-AuNPs.

corresponding to the peak at 543 nm. Reported that gold nanoparticles have an absorbance peak between 500 and 550 nm depending on the particle size [28]. The figure shows that the reaction was started at 5 min and completed in 80 min.

FTIR was used to examine the change of compound functional groups after reacted with gold ion during nanomization. Fig. 2 shows strong peak which was assigned to −OH stretching appeared at 3419.87 cm^{-1} in LA became sharper and higher in intensity at 3431.36 cm^{-1} in LA-AuNPs spectrum [29]. The vibrational stretching of aliphatic -CH- was found to exhibit at 2929.87 cm^{-1} in LA, and around 2922.16 cm^{-1} in LA-AuNPs [30]. The reduced band at 1734.01 cm^{-1} which belonged to the -C=O ester in LA was shifted to 1739.79 cm^{-1} in LA-AuNPs spectrum. This indicates the elimination of the terminal esteric group, followed by the reduction of -OH to -C=O**.** The other minor bands at 1647.21 cm^{-1} in LA and 1633.71 cm^{-1} in LA-AuNPs, were found to correspond to the carbonyl group -C=O [31]. The spikes at 1286.52 cm^{-1} and 1074.35 cm^{-1} correspond to the C-O-C and -CO of the aromatic ester and primary alcohol, respectively. Those bands were reduced as appeared at 1265.30 cm^{-1} and 1070.49 cm^{-1} in LA-AuNPs spectrum.

3.2. Determination of elemental composition by EDX

The elements in the synthesized LA-AuNPs were determined using EDX. The strongest peak of gold was noticed around 2.2 keV, in addition to another two minor peaks located at 8.5 and 9.7, respectively (Fig. 3(b)). This indicates that gold as the predominant element with the total weight of 48.6%. The other low intense peaks such as, O, Na, Si, S, Cl, P, Ni, Al, Mg and K were also identified (Fig. 3(a)). The existence of Si signal was most probably leached from glass during sample preparation.

3.3. Crystallographic structure of LA-AuNPs

XRD measurement was used to examine the crystalline structure of the synthesized LA-AuNPs (Fig. 4). A number of Bragg reflections which is categorized as the face-centered cubic structure of gold can be seen from the figure. The strongest peaks were assigned to the diffractions at 2θ; 38.417° (111), 44.603° (200), 64.725° (220) and 77.618° (311) which was identical with the data reported for the standard gold metal (Joint Committee on Powder Diffraction Standards, no. 04−0784, USA). The mean of crystallite size was found to be 29.5 ± 5.49 nm. This explains the cubic

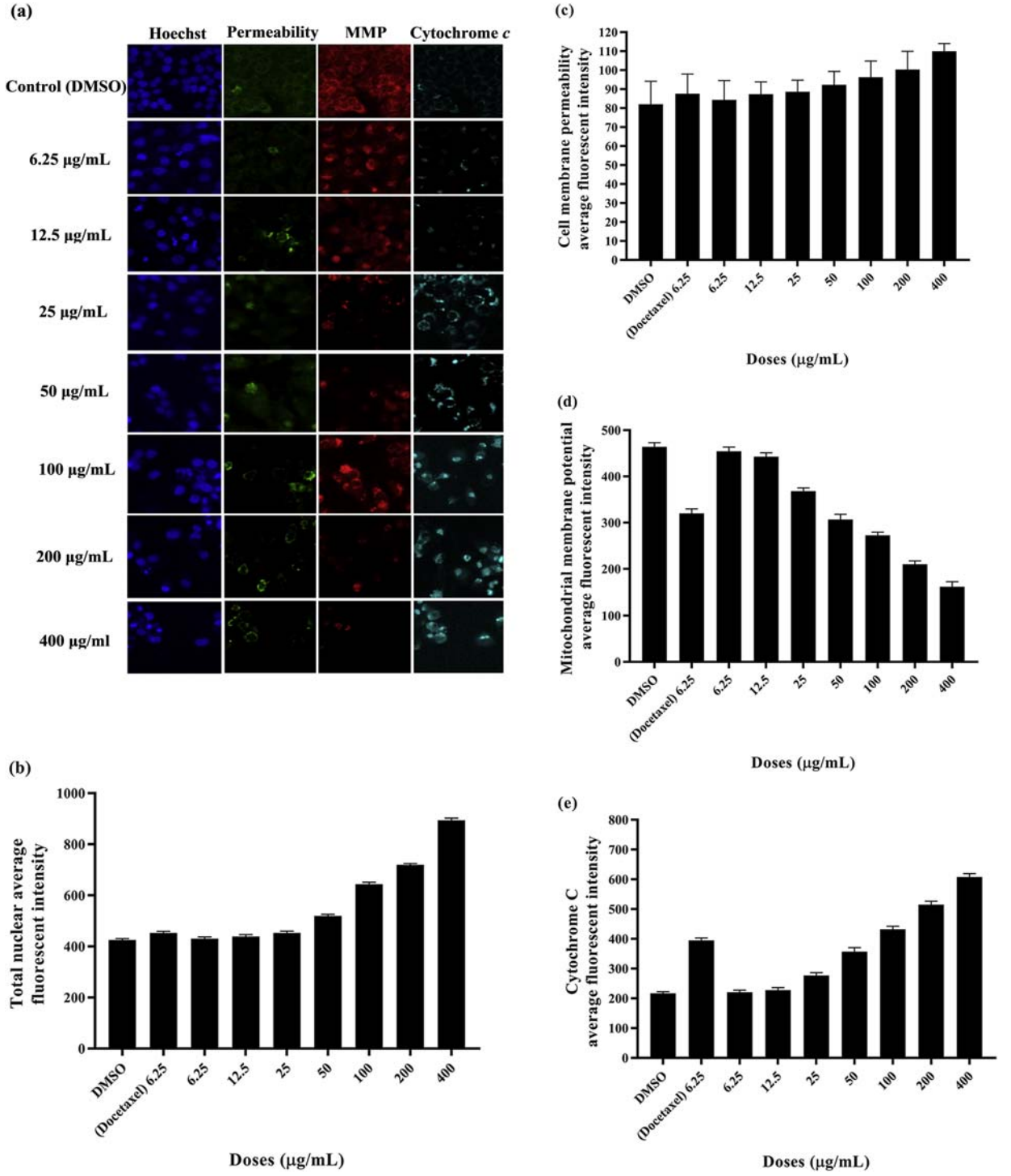

Fig. 8. Effect of LA-AuNPs on nuclear intensity, membrane permeability, MMP and cytochrome c, (a) representative images of LA-AuNPs treated and untreated LNCaP cells, stained with hoechst 33,342 for nuclear, membrane permeability, MMP and cytochrome *c* dyes, in which the quantitative information is explained in the bar charts of (b) nuclear intensity, (c) cell permeability, (d) MMP, and (e) cytochrome c release, respectively.

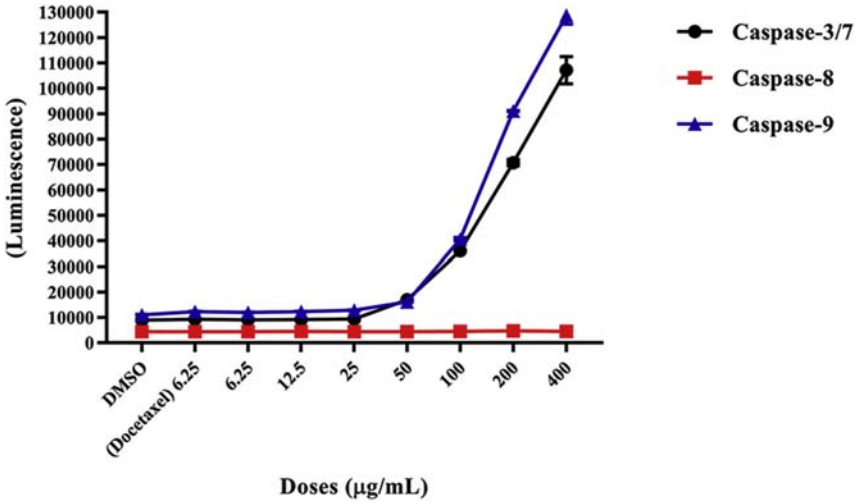

Fig. 9. Effect of LA-AuNPs on caspases −3/7, −8 and −9 activities.

structure of metallic gold and the crystallinity of LA-AuNPs (Ramkumar et al.) [20].

3.4. Surface morphology of synthesized LA-AuNPs

The particle size distribution of synthesized LA-AuNPs was determined based on the principle of dynamic light scattering. Particle size was determined by measuring the random changes in the intensity of light scattered from a solution. Fig. 5 shows the hydrodynamic average size of 67.94 ± 1.76 nm for LA-AuNPs with the polydispersity index (PDI) of 0.381. The results explained the medium mono-dispersity with minimal aggregation of nanoparticles. The electrical charge on the particles was contributed by functional groups on the surface of particles. The zeta potential of LA-AuNPs was −30.11 ± 0.83 mV which was considered to be physically stable [31]. The zeta potential explains the stability of nanoparticles stability in colloidal solution.

Another three analytical techniques such as AFM, FESEM and TEM were used to describe the morphology of the synthesized LA-AuNPs. AFM is a powerful tool to examine the morphological features of LA-AuNPs in a 3D micrograph as presented in Fig. 6(a). The AFM image displays the nearly spherical topology of nanoparticles with the mean particles size about 59.86 nm. The FESEM result was in line with the topological image generated by AFM. Fig. 6(b) also reveals the approximately spherical shape of synthesized LA-AuNPs in a homogeneous distribution with the mean particles size of 63.59 ± 20.502 nm (Fig. 6(c)). Further morphological observation was monitored using TEM. Fig. 6(d) exhibits the spherical allographic structure of nanoparticles with the mean particles size of 62.40 ± 14.022 nm. All morphological studies indicated the spherical and nano-sized particles (59.86–67.94 nm) were successfully produced in this study.

3.5. Cytotoxicity of LA-AuNPs

The MTT assay was used to measure the cytotoxic activity of the synthesized LA-AuNPs against LNCaP and RWPE-1 cells. LNCaP cells displayed the decrease of cell viability after 24 h of treatment, especially at the concentration higher than 50 µg/mL. LA-AuNPs were found to be non-toxic to RWPE-1 cells compared to the minimum selective concentration of drug (docetaxel) as presented in Fig. 7. The IC50 was presented to be 126.82 µg/mL for LNCaP cells, whereas 705.56 µg/mL for RWPE-1 cells. Hence, LA-AuNPs have a potent anti-cancer activity against cancer cells and non-toxic for normal cells [32]. This cytotoxicity could be attributed to the physiochemical interaction of gold and LA with the functional groups of intracellular proteins, as well as with the nitrogen bases and phosphate groups in DNA [33]. Lee et al. [34] reported that the magnitude of surface charge is not an exclusive factor to determine the cytotoxicity of gold nanoparticles. The cytotoxicity was mostly probably due to the hydrophobic moiety which induced the lytic interaction with plasma membrane. This phenomenon would hinder cell proliferation by slowing down cell migration, inhibiting DNA replication and causing DNA damage. Of late, Ramkumar et al. [20] reported the synthesis of LA-AuNPs using the root extract of *L.*

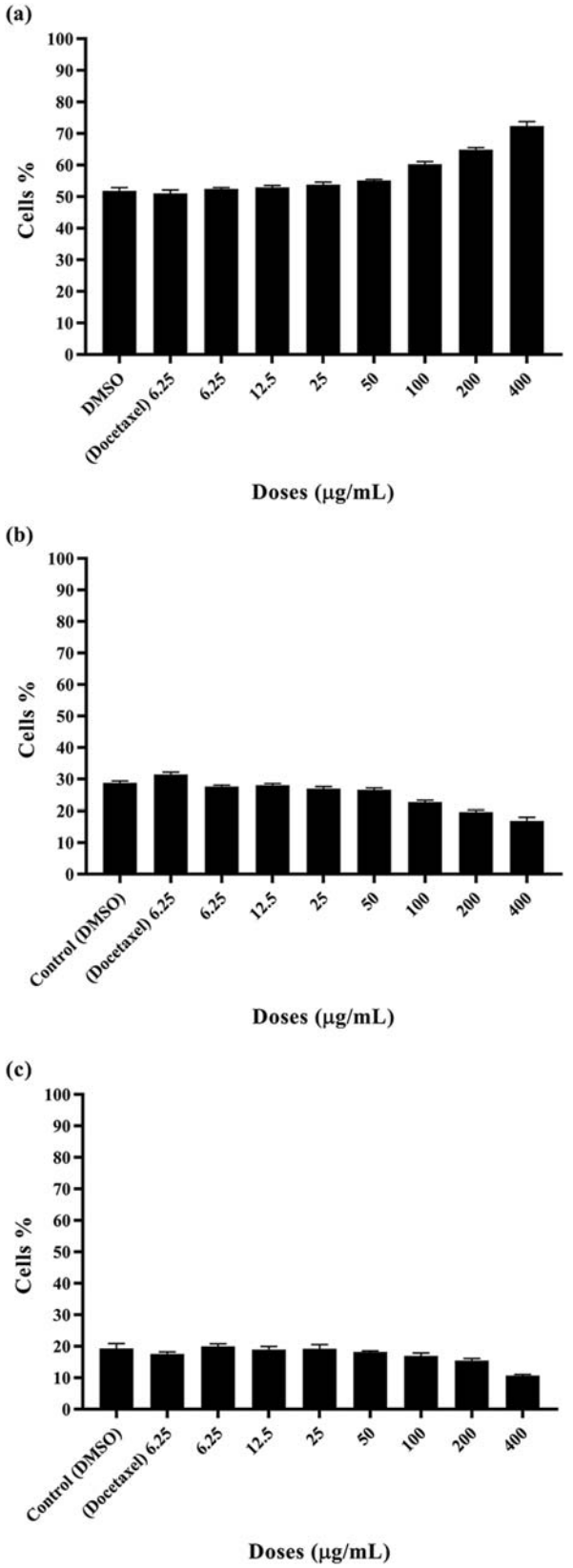

Fig. 10. The cell cycle phases of (a) G0/G1, (b) S and (c) G2/M.

camara. The cytotoxic activity was assessed against MBA-MB-231 breast cancer and Vero normal cells. They also revealed that the plant extract loaded nanoparticles showed a selective toxicity against MBA-MB-231 breast cancer cells rather than Vero normal cells [20]. The finding explained the non-toxicity of gold nanoparticles to normal cell lines.

3.6. High content screening (HCS) assay

The apoptosis or survival of cells are mostly regulated and controlled by mitochondria. Therefore, any disturbances on cell nuclear, cell membrane permeability, MMP and regulation of caspases could result to cell death [35]. Therefore, the treated LNCaP cells were assessed using HCS. The blue intensity of Hoechst dye was increased with the increased concentration of LA-AuNPs in cancer cell treatment (Fig. 8(a)). The increment was significant at the concentration ranged from 50 to 400 µg/mL. The increase of nuclear fragmentation was observed at higher concentration of LA-AuNPs in comparison to control as shown in Fig. 8(b). Fig. 8(c) shows to have a slight increment in the permeability of cell membrane. However, the treated LNCaP cells were weakly stained with MMP dye in comparison to untreated cells. The LA-AuNPs also induced a dose-dependent disturbance in MMP as shown in Fig. 8(c). Approximately, 50 µg/mL of LA-AuNPs was equal to the performance of docetaxel (6.25 µg/mL) in reducing MMP. Meanwhile, the collapse of (MMP) lead to the elevation in releasing of cytochrome C to cytosols (Fig. 8 (d)). We supposed the LA-AuNPs could induce apoptosis by targeting the mitochondria and its contents [36].

3.7. LA-AuNPs induced caspase −3/7, 8 and −9 activities

Caspases are a group of cysteine proteolytic enzymes which can be used to determine apoptosis pathway [37]. Thus, the activity of caspase −3/7, −8, and −9 in LNCaP cells were monitored after LA-AuNPs administration for 24 h. As shown in Fig. 9, LA-AuNPs induced a dose-dependent increment in caspases −3/7 and −9 activities starting from 50 to 400 µg/mL. In contrast, there is almost no significant change of caspase-8 activity. The intrinsic mechanism of mitochondria involved the activation of caspase-3 and -9 which were mostly regulated by Bcl-2 family proteins [38]. Bcl-2 protein was downregulated and Bax was transferred into mitochondria, and thus leading to the collapse of MMP to release cytochrome C

[39]. The cytochrome C forms a complex with Apaf-1 which is called apoptosome. Apoptosome would lead to the activation of caspase-9, and consequently the activation of caspase-3/7 in apoptosis [40]. The LA-AuNPs induced caspases-3/7 and −9 activation, but did not activate caspase-8. Therefore, LA-AuNPs followed the mitochondrial intrinsic pathway of apoptosis.

3.8. Cell cycle arrest analysis

The antiproliferation of cells can be explained by cell cycle arrest using a flow cytometer [41]. As shown in Fig. 10, the percentage of cell count was substantially increased with the increase of LA-AuNPs concentration in the G0/G1 phase compared to the cell count of control. The treatment was significant ($P < 0.05$) at the concentration of 25−400 μg/mL. Controversially, the cells population in the S and G2/M phases was substantially lower than that of control. The lack of control in cell cycle always results in cancer development [42]. The cyclin-dependent kinases (CDKs) regulated the progression of cell cycle via the interaction between regulatory sub-unit (cyclin) and cyclin-dependent kinase inhibitors (CDKIs) [43−45]. However, the activities of CDKs are specific to the various stages of cell cycle. The G1 phase progression is mediated by CDK4 and CDK6 and complexed with D-type cyclins [46]. The G1-S phase transition may regulate by CDK2-cyclin E complexes, while a complex CDK2-cyclin A was responsible for S phase progression. The transition of G2-M phase is controlled by CDK1-cyclin B [47,48]. It is known that anti-tumor agent may induce cell cycle arrest at the G1, S, or G2/M phases [50]. In the present study, LA-AuNPs induced a dose-dependent cell cycle arrest in LNCaP cells at the G0/G1 phase.

4. Conclusion

A simple, cost-effective and eco-friendly method for the synthesis of LA-AuNPs was successfully carried out. Gold (III) ion was chemically reduced to gold using LA as a reducing agent. FTIR revealed that the stabilization of gold ions by LA through the bio-reduction of esteric groups. The mean particles size was 67.94 ± 1.76 nm with medium monodispersity and high stability of nanoparticles in colloid. The spherical shape of synthesized LA-AuNPs was cytotoxic to prostate cancer cells but non-toxic to normal prostate cells. LA-AuNPs induced intrinsic apoptosis via the activation of caspases −3/7 and −9 and stimulated the cell cycle arrest at the G0/G1 phase. Hence, the synthesized LA-AuNPs have therapeutic potential in prostate cancer therapy.

References

[1] R.K. Jha, P.K. Jha, K. Chaudhury, S.V. Rana, S.K. Guha, An emerging interface between life science and nanotechnology: present status and prospects of reproductive healthcare aided by nano-biotechnology, Nano Rev. 5 (2014) 22762, https://doi.org/10.3402/nano.v5.22762.

[2] S. Wang, T. Chen, R. Chen, Y. Hu, M. Chen, Y. Wang, Emodin loaded solid lipid nanoparticles: preparation, characterization and antitumor activity studies, Int. J. Pharm. 430 (2012) 238−246, https://doi.org/10.1016/j.ijpharm.2012.03.027.

[3] D. Mandal, M.E. Bolander, D. Mukhopadhyay, G. Sarkar, P. Mukherjee, The use of microorganisms for the formation of metal nanoparticles and their application, Appl. Microbiol. Biotechnol. 69 (2006) 485−492, https://doi.org/10.1007/s00253-005-0179-3.

[4] B. Bhattarai, Y. Zaker, T.P. Bigioni, Green synthesis of gold and silver nanoparticles: challenges and opportunities, Curr. Opin. Green Sustain. Chem. 12 (2018) 91−100, https://doi.org/10.1016/j.cogsc.2018.06.007.

[5] N. Savithramma, M.L. Rao, K. Rukmini, P.S. Devi, Antimicrobial activity of silver nanoparticles synthesized by using medicinal plants, Int. J. ChemTech Res. 3 (2011) 1394−1402.

[6] N. Suganthy, V. Sri Ramkumar, A. Pugazhendhi, G. Benelli, G. Archunan, Biogenic synthesis of gold nanoparticles from Terminalia arjuna bark extract: assessment of safety aspects and neuroprotective potential via antioxidant, anticholinesterase, and antiamyloidogenic effects, Environ. Sci. Pollut. Res. Int. 25 (2018) 10418−10433, https://doi.org/10.1007/s11356-017-9789-4.

[7] S.S. Shankar, A. Rai, A. Ahmad, M. Sastry, Rapid synthesis of Au, Ag, and bimetallic Au core−Ag shell nanoparticles using Neem (Azadirachta indica) leaf broth, J. Colloid Interface Sci. 275 (2004) 496−502, https://doi.org/10.1016/j.jcis.2004.03.003.

[8] M. Rai, A. Yadav, A. Gade, CRC 675—current trends in phytosynthesis of metal nanoparticles, Crit. Rev. Biotechnol. 28 (2008) 277−284, https://doi.org/10.1080/07388550802368903.

[9] R. Geetha, T. Ashokkumar, S. Tamilselvan, K. Govindaraju, M. Sadiq, G. Singaravelu, Green synthesis of gold nanoparticles and their anticancer activity, Cancer Nanotechnol. 4 (2013) 91−98, https://doi.org/10.1007/s12645-013-0040-9.

[10] A. Sett, M. Gadewar, P. Sharma, M. Deka, U. Bora, Green synthesis of gold nanoparticles using aqueous extract of Dillenia indica, Adv. Nat. Sci. Nanosci. Nanotechnol. 7 (2016), 025005, https://doi.org/10.1088/2043-6262/7/2/025005.

[11] A. Ahmad, F. Syed, M. Imran, A.U. Khan, K. Tahir, Z.U.H. Khan, Q. Yuan, Phytosynthesis and antileishmanial activity of gold nanoparticles by M aytenus Royleanus, J. Food Biochem. 40 (2016) 420−427, https://doi.org/10.1111/jfbc.12232.

[12] S. Vijayakumar, B. Vaseeharan, B. Malaikozhundan, N. Gopi, P. Ekambaram, R. Pachaiappan, P. Velusamy, K. Murugan, G. Benelli, R.S. Kumar, Therapeutic effects of gold nanoparticles synthesized using Musa paradisiaca peel extract

against multiple antibiotic resistant Enterococcus faecalis biofilms and human lung cancer cells (A549), Microb. Pathog. 102 (2017) 173–183, https://doi.org/10.1016/j.micpath.2016.11.029.

[13] K. Xin Lee, K. Shameli, M. Miyake, N. Kuwano, N.B. Bt Ahmad Khairudin, S.E. Bt Mohamad, Y.P. Yew, Green synthesis of gold nanoparticles using aqueous extract of Garcinia mangostana fruit peels, J. Nanomater. 2016 (2016), https://doi.org/10.1155/2016/8489094.

[14] R.B. Hurtado, M. Cortez-Valadez, L. Ramírez-Rodríguez, E. Larios-Rodriguez, R.A. Alvarez, O. Rocha-Rocha, Y. Delgado-Beleño, C. Martinez-Nuñez, H. Arizpe-Chávez, A. Hernández-Martínez, Instant synthesis of gold nanoparticles at room temperature and SERS applications, Phys. Lett. 380 (2016) 2658–2663, https://doi.org/10.1016/j.physleta.2016.05.052.

[15] M. Mavukkandy, S. Chakraborty, T. Abbasi, S. Abbasi, A clean-green synthesis of platinum nanoparticles utilizing a pernicious weed lantana (Lantana Camara), Am. J. Eng. Appl. Sci. 9 (2016) 84–90, https://doi.org/10.3844/ajeassp.2016.84.90.

[16] B. Kumar, K. Smita, L. Cumbal, Biosynthesis of silver nanoparticles using Lantana camara flower extract and its application, J. Sol. Gel Sci. Technol. 78 (2016) 285–292, https://doi.org/10.1007/s10971-015-3941-8.

[17] V. Manjamadha, K. Muthukumar, Ultrasound assisted green synthesis of silver nanoparticles using weed plant, Bioproc. Biosyst. Eng. 39 (2016) 401–411, https://doi.org/10.1007/s00449-015-1523-3.

[18] S.S. Dash, B.G. Bag, P. Hota, Lantana camara Linn leaf extract mediated green synthesis of gold nanoparticles and study of its catalytic activity, Appl. Nanosci. 5 (2015) 343–350, https://doi.org/10.1007/s13204-014-0323-4.

[19] B. Kumar, K. Smita, L. Cumbal, A. Debut, Extracellular biofabrication of gold nanoparticles by using Lantana camara berry extract, Inorgan. Nano-Metal Chem. 47 (2017) 138–142, https://doi.org/10.1080/15533174.2016.1157817.

[20] R. Ramkumar, G. Balasubramani, R.K. Raja, M. Raja, R. Govindan, E.K. Girija, P. Perumal, Lantana camara Linn root extract-mediated gold nanoparticles and their in vitro antioxidant and cytotoxic potentials, Artificial cells, Nanomed. Biotechnol. 45 (2017) 748–757, https://doi.org/10.1080/21691401.2016.1276923.

[21] O.P. Sharma, H.P. Makkar, R.K. Dawra, A review of the noxious plant Lantana camara, Toxicon 26 (1988) 975–987, https://doi.org/10.1016/0041-0101(88)90196-1.

[22] D. Ganjewala, S. Sam, K.H. Khan, Biochemical compositions and antibacterial activities of Lantana camara plants with yellow, lavender, red and white flowers, EurAsia J. BioSci. 3 (2009) 69–77, https://doi.org/10.5053/ejobios.2009.3.0.10.

[23] M. Sharma, P. Sharma, Optimization of lantadenes isolation and preparation of 22 β-hydroxyoleanonic acid, Chem. Nat. Compd. 42 (2006) 442–444, https://doi.org/10.1007/s10600-006-0176-5.

[24] O.P. Sharma, A. Singh, S. Sharma, Levels of lantadenes, bioactive pentacyclic triterpenoids, in young and mature leaves of Lantana camara var. aculeata, Fitoterapia 71 (2000) 487–491, https://doi.org/10.1016/s0367-326x(00)00156-8.

[25] R. Geethalakshmi, D. Sarada, Characterization and antimicrobial activity of gold and silver nanoparticles synthesized using saponin isolated from Trianthema decandra L, Ind. Crop. Prod. 51 (2013) 107–115, https://doi.org/10.1016/j.indcrop.2013.08.055.

[26] K. Gopinath, S. Kumaraguru, K. Bhakyaraj, S. Mohan, K.S. Venkatesh, M. Esakkirajan, P. Kaleeswarran, N.S. Alharbi, S. Kadaikunnan, M. Govindarajan, Green synthesis of silver, gold and silver/gold bimetallic nanoparticles using the Gloriosa superba leaf extract and their antibacterial and antibiofilm activities, Microb. Pathog. 101 (2016) 1–11, https://doi.org/10.1016/j.micpath.2016.10.011.

[27] J.K. Patra, K.-H. Baek, Green nanobiotechnology: factors affecting synthesis and characterization techniques, J. Nanomater. 2014 (2014), https://doi.org/10.1155/2014/417305.

[28] D.M. Gindri, C.M.M. Coelho, V.G. Uarrota, A.M. Rebelo, Herbicidal bioactivity of natural compounds from Lantana camara on the germination and seedling growth of Bidens pilosa, Pesqui. Agropecuária Trop. 50 (2020), https://doi.org/10.1590/1983-40632020v5057746.

[29] G.S. Ingawale, A.S. Goswami-Giri, Isolation and characterization of bioactive molecule from Lantana camara, Asian J. Res. Chem. 7 (2014) 339.

[30] P. Sivakumar, C. Nethradevi, S. Renganathan, Synthesis of silver nanoparticles using Lantana camara fruit extract and its effect on pathogens, Asian J. Pharmaceut. Clin. Res. 5 (2012) 97–101.

[31] M. Faried, K. Shameli, M. Miyake, A. Hajalilou, K. Kalantari, Z. Zakaria, H. Hara, N.B.A. Khairudin, Synthesis of silver nanoparticles via green method using ultrasound irradiation in seaweed Kappaphycus alvarezii media, Res. Chem. Intermed. 42 (2016) 7991–8004, https://doi.org/10.1007/s11164-016-2574-z.

[32] R. Vijayan, S. Joseph, B. Mathew, Indigofera tinctoria leaf extract mediated green synthesis of silver and gold nanoparticles and assessment of their anticancer, antimicrobial, antioxidant and catalytic properties, Artificial cells, Nanomed. Biotechnol. 46 (2018) 861–871, https://doi.org/10.1080/21691401.2017.1345930.

[33] A.M. Hunter, E.C. LaCasse, R.G. Korneluk, The inhibitors of apoptosis (IAPs) as cancer targets, Apoptosis 12 (2007) 1543–1568, https://doi.org/10.1007/s10495-007-0087-3.

[34] N. Ajenjo, E. Canon, I. Sanchez-Perez, D. Matallanas, J. Leon, R. Perona, P. Crespo, Subcellular localization determines the protective effects of activated ERK2 against distinct apoptogenic stimuli in myeloid leukemia cells, J. Biol. Chem. 279 (2004) 32813–32823, https://doi.org/10.1074/jbc.M313656200.

[35] E.S. Alnemri, D.J. Livingston, D.W. Nicholson, G. Salvesen, N.A. Thornberry, W.W. Wong, J. Yuan, Human ICE/CED-3 protease nomenclature, Cell 87 (1996) 171, https://doi.org/10.1016/s0092-8674(00)81334-3.

[36] M.H. Kang, C.P. Reynolds, Bcl-2 inhibitors: targeting mitochondrial apoptotic pathways in cancer therapy, Clin. Cancer Res. 15 (2009) 1126–1132, https://doi.org/10.1158/1078-0432.CCR-08-0144.

[37] Y. Tsujimoto, Role of Bcl-2 family proteins in apoptosis: apoptosomes or mitochondria? Gene Cell. 3 (1998) 697–707, https://doi.org/10.1046/j.1365-2443.1998.00223.x.

[38] G.M. Cohen, Caspases: the executioners of apoptosis, Biochem. J. 326 (Pt 1) (1997) 1–16, https://doi.org/10.1042/bj3260001.

[39] L. Ma, G.B. Xu, X. Tang, C. Zhang, W. Zhao, J. Wang, H. Chen, Anti-cancer potential of polysaccharide extracted

from hawthorn (Crataegus.) on human colon cancer cell line HCT116 via cell cycle arrest and apoptosis, J. Funct. Foods 64 (2020) 103677, https://doi.org/10.1016/j.jff.2019.103677.

[40] K.I. Nakayama, K. Nakayama, Ubiquitin ligases: cell-cycle control and cancer, Nat. Rev. Cancer 6 (2006) 369−381, https://doi.org/10.1038/nrc1881.

[41] M. Molinari, Cell cycle checkpoints and their inactivation in human cancer, Cell Prolif 33 (2000) 261−274, https://doi.org/10.1046/j.1365-2184.2000.00191.x.

[42] M.B. Kastan, Q. Zhan, W.S. El-Deiry, F. Carrier, T. Jacks, W.V. Walsh, B.S. Plunkett, B. Vogelstein, A.J. Fornace Jr., A mammalian cell cycle checkpoint pathway utilizing p53 and GADD45 is defective in ataxia-telangiectasia, Cell 71 (1992) 587−597, https://doi.org/10.1016/0092-8674(92)90593-2.

[43] C.J. Sherr, J.M. Roberts, CDK inhibitors: positive and negative regulators of G1-phase progression, Genes Dev. 13 (1999) 1501−1512, https://doi.org/10.1101/gad.13.12.1501.

[44] C.J. Sherr, Mammalian G1 cyclins, Cell 73 (1993) 1059−1065, https://doi.org/10.1016/0092-8674(93)90636-5.

[45] A.M. Senderowicz, E.A. Sausville, Preclinical and clinical development of cyclin-dependent kinase modulators, J. Natl. Cancer Inst. 92 (2000) 376−387, https://doi.org/10.1093/jnci/92.5.376.

[46] X. Graña, E.P. Reddy, Cell cycle control in mammalian cells: role of cyclins, cyclin dependent kinases (CDKs), growth suppressor genes and cyclin-dependent kinase inhibitors (CKIs), Oncogene 11 (1995) 211−220.

[47] C.J. Sherr, The Pezcoller lecture: cancer cell cycles revisited, Cancer Res. 60 (2000) 3689−3695.

[48] A. Gomes, B. Giri, A. Alam, S. Mukherjee, P. Bhattacharjee, A. Gomes, Anticancer activity of a low immunogenic protein toxin (BMP1) from Indian toad (Bufo melanostictus, Schneider) skin extract, Toxicon 58 (2011) 85−92, https://doi.org/10.1016/j.toxicon.2011.05.008.